The PD-1 Axis Enforces an Anatomical Segregation of CTL Activity that Creates Tumor Niches after Allogeneic Hematopoietic Stem Cell Transplantation

David Michonneau, Pervinder Sagoo, Béatrice Breart, Zacarias Garcia, Susanna Celli, Philippe Bousso

The PD-1 axis enforces an anatomical segregation of CTL activity that creates tumor niches after allogeneic hematopoietic stem cell transplantation

David Michonneau[1,2,3], Pervinder Sagoo[1,2], Béatrice Breart[1,2], Zacarias Garcia[1,2], Susanna Celli[1,2,4] and Philippe Bousso[1,2,4]

[1]Institut Pasteur, Dynamics of Immune Responses Unit, Equipe Labéllisée Ligue Contre le Cancer, 75015 Paris, France.

[2]INSERM U668, rue du Dr Roux, 75015 Paris, France.

[3]University Paris Diderot, Sorbonne Paris Cité, Cellule Pasteur, rue du Dr Roux, 75015 Paris, France.

[4]These authors contributed equally to this work

Correspondence to: philippe.bousso@pasteur.fr

Allogeneic hematopoietic stem cell transplantation (allo-HSCT), a curative treatment for hematologic malignancies relies on donor cytotoxic T lymphocyte (CTL)-mediated graft-versus-leukemia (GVL) effect. Major complications of HSCT are graft-versus-host disease (GVHD) that targets specific tissues and tumor relapses. However, the mechanisms dictating the anatomical features of GVHD and GVL remain unclear. Here, we show that after HSCT, CTLs exhibited different killing activity in distinct tissues, being highest in the liver and lowest in lymph nodes. Differences were imposed by the microenvironment, partly through differential PD-1 ligands expression, which was strongly elevated in lymph nodes. Two-photon imaging revealed that PD-1 blockade restored CTL sensitivity to antigen and killing in lymph nodes. Weak CTL activity in lymph nodes promoted local tumor escape but could be reversed by anti-PD-1 treatment. Our results uncover a mechanism generating an anatomical segregation of CTL activity that may dictate sites of GVHD and create niches for tumor escape.

Allogeneic hematopoietic stem cell transplantation (allo-HSCT) is a major curative treatment for patients with hematologic malignancies, which aims to induce a graft-versus-leukemia (GVL) effect to eliminate residual tumor cells in host. Most allo-HSCTs are now performed in the context of HLA compatible donors (Gratwohl et al., 2013) with a GVL reaction being mediated by donor T cells reacting against host minor histocompatibility antigens (miHAg) (Goulmy et al., 1996). However, allo-HSCT is still hampered by a high mortality rate, largely due to tumor relapse and graft-versus-host disease (GVHD) (Pasquini et al., 2013). While most miHAgs are broadly expressed in tissues, GVHD preferentially affects organs such as the liver, the gut and the skin (Ferrara et al., 2009). These anatomical features have been imputed to the homing properties of effector T cells (Sackstein, 2006), local inflammation induced by the conditioning regimen (Chakraverty, 2006; Wilhelm et al., 2010) or to tissue-specific sensitivity to cytotoxic T lymphocyte (CTL)-mediated killing (Vincent et al., 2011).

Relapse after allo-HSCT reflects the failure of the GVL reaction to eliminate all residual malignant cells. The tumor may escape the GVL reaction through the selection of variant clones resistant to the immune response (Dermime et al., 1997; Matte-Martone et al., 2011). Additionally, the GVL reaction may become less efficient over time due to the progressive dampening of donor T cell activity. During allo-HSCT, donor T cell activity can be suppressed by regulatory T cells and NKT cells (Schneidawind et al., 2013) or through expression of co-inhibitory receptors such as PD-1 (Blazar et al., 2003), Tim-3 (Veenstra et al., 2012), Lag-3 (Sega et al., 2014) or Vista (Flies et al., 2011). Interestingly, relapses after allo-HSCT occur more frequently at extramedullary sites than relapses after chemotherapy only (Shimizu et al., 2013). These observations raise the possibility that, similar to GVHD, the GVL effect may not be exerted uniformly in all organs. Addressing this question is of critical importance to clarify how residual tumor cells may escape the immune surveillance mediated by donor T cells after HSCT.

Using a model of single miHAg-mismatched HSCT, we demonstrate here that the activity of CTLs varied extensively between organs. This heterogeneity was imposed, at least partly, by the distinct expression of PD-1 ligands encountered in different tissue microenvironments that regulate T cell sensitivity to antigen. Finally, we provide evidence that such spatially compartmentalized CTL activity created niches for tumor escape after HSCT.

Our results support the idea that both GVHD and GVL are subjected to a stringent anatomical compartmentalization due to the local tuning of T cell activity imposed by the tissue microenvironment.

Results

A model of HSCT transplantation based on H-Y mismatch induces GVHD

To study CTL activity in the context of allo-HSCT, we relied on a mouse model based on H-Y minor histocompatibility mismatch (we will use the conventional terminology for allo-HSCT, i.e. non syngeneic transplants). In this setting, T cell-depleted female bone marrow (BM) cells, $CD8^+$ T cells expressing the anti-H-Y MataHari TCR (that recognizes a Db-restricted peptide derived from the male *Uty* gene) and polyclonal $CD4^+$ T cells (to provide T cell help (Bourgeois et al., 2002)) were adoptively transferred into lethally irradiated male recipients (**Fig. 1A**). As a control, the same procedure was applied to female recipients that lack the cognate antigen for MataHari T cells. Transplanted male recipients developed a sub-lethal GVHD as measured by clinical scoring (Cooke et al., 1996) (**Fig. 1B**). No GVHD was detected in transplanted female recipients or in male recipients receiving only BM cells (without MataHari T cells). The GVHD developed by male recipients was characterized by a potent infiltration of H-Y-specific T cells in the liver, gut and skin (**Fig. 1C, Fig. S1**). As expected, these typical hallmarks of GVHD were absent in female recipients (that lack H-Y antigens). T cell infiltration was associated with tissue destruction as we detected cell apoptosis in the liver of male recipients (**Fig. 1D**). Apoptotic cells included hepatocytes (identified by their typical morphology) and were localized in CTL rich areas (**Fig. 1E**). This experimental setting therefore provided us with a model of HSCT that induced a mild, sub-lethal GVHD similar to that elicited in human patients after miHAg-mismatched HSCT.

Anatomical segregation of CTL activity during allo-HSCT

The fact that specific organs (including liver, gut and skin) are preferentially targeted during GVHD raises the possibility that these tissues are intrinsically more sensitive to CTL-induced

killing (e.g due to higher alloantigen expression). Alternatively, CTLs may exhibit distinct cytotoxic potential at different anatomical sites. To test the latter hypothesis, we first sought to measure *in vivo* killing of transferred cell targets in different organs. H-Y is broadly expressed in tissues but subtle differences may potentially exists between organs. The use of transferred target cells allowed us to compare the intrinsic activity of CTLs in different locations, irrespective of the target properties. To this end, male recipients transplanted with bone marrow and MataHari $CD8^+$ T cells received a mixture of male and female splenocytes labeled with high and low concentration of CFSE, respectively. Killing of male target cells by MataHari T cells was quantified 36 hours later by flow cytometry (**Fig. 2A**). A comparison was performed between male and female recipients to highlight the contribution of chronic exposure to antigen mismatch on CTL activity. In control transplanted female recipients, injected male splenocytes were effectively killed in all organs tested (**Fig. 2B**). Thus, in this setting of syngeneic HSCT, MataHari T cells become activated (through lymphopenia-induced proliferation and/or recognition of targets) and efficiently killed transferred male targets. Strikingly, in male recipients, we only observed target cell killing in the liver but not in lymph nodes, spleen or bone marrow (**Fig. 2B**). The absence of killing in these sites in male recipients was not due to poor CTL infiltration as male displayed higher frequency of MataHari $CD8^+$ T cells and higher effector:target ratios in these organs compared to female recipients (**Fig. S2**). These observations suggested that miHAg mismatch during HSCT results in a dampening of CTL killing activity in lymphoid organs. To more directly assess the lack of *in situ* CTL killing in the lymphoid organs of transplanted male recipients, we visualized target cell death in lymph nodes by intravital two-photon imaging. Male splenocytes were used as targets and were labeled with a combination of a cytoplasmic and nuclear dye, an approach previously described to monitor cell death by a change of dye fluorescence ratio (Mempel et al., 2006) (**Fig. 2C**). Again, we observed numerous dead target

cells in the lymph nodes of control female recipients (characterized by a low fluorescence ratio and absence of motility), but a virtually complete lack of killing in male recipients (**Fig. 2D-E**). Altogether, these experiments established the existence of an anatomical compartmentalization of host-reactive CTLs during HSCT.

$CD8^+$ T cell cytotoxic phenotype is modulated in specific microenvironments

The spatial segregation of CTL activity observed during allo-HSCT may result from the selective migration of CTLs with the highest killing potential to specific peripheral organs such as the liver. An alternative explanation would be that the cytotoxic potential of CTLs is locally regulated in specific microenvironments. To distinguish between these two possibilities, we thought to assess if the cytotoxic phenotype of individual CTLs is intrinsic to the cell or may vary depending on the environment.

First, in good agreement with our killing assay, we found that CTLs present in male transplanted mice expressed high amounts of granzyme B in the liver (and in other GVHD target organs such as gut and skin) but low amounts in lymph nodes, spleen and bone marrow (**Fig. 3A**). For further study, we chose to dissect CTL activity in lymph nodes versus liver, two sites containing large numbers of CTLs but with contrasting *in situ* cytotoxic activity. In addition, these two organs can be infiltrated by hematologic malignancies and are therefore relevant for studying GVL efficiency. We asked if lymph node and liver CTLs that displayed low and high granzyme B expression, respectively, would migrate to their original location and maintain their phenotype upon transfer into a distinct transplanted recipient (**Fig. 3B**). We found that transferred CTLs migrated to various organs, including lymph nodes, spleen, bone marrow, liver and gut, irrespective of their origin (**Fig. S3**). Most importantly, CTLs isolated from the liver that migrated to the lymph node, the spleen or the bone-marrow after transfer, had lost granzyme B expression. Conversely, lymph node-derived CTLs that migrated to the

liver or the gut acquired elevated granzyme B levels (**Fig. 3C, D**). In summary, the differential CTL phenotype seen in distinct organs does not appear to be the result of selective migration processes. Instead, our results support the idea that organ-specific microenvironments dictate CTL cytotoxic potential during allo-HSCT.

The CTL activity in lymph nodes during allo-HSCT is dampened by the PD-1 pathway

One hallmark of allo-HSCT is that reactive T cells are chronically exposed to host antigens, a feature that may lead to functional exhaustion. Consistent with previous studies in mice (Asakura et al., 2010; Flutter et al., 2010; Koestner et al., 2011) and humans (Norde et al., 2011), we found the inhibitory receptor PD-1 to be upregulated on MataHari $CD8^+$ T cells in male transplanted mice but not in control females (**Fig. 4A**). This phenomenon was detected in all the organs tested, indicating that, PD-1 upregulation alone could not account for the spatial compartmentalization of CTL activity observed. This prompted us to also analyze the expression of PD-1 ligands in distinct organs. We found that HSCT induced a marked elevation of both PD-L1 and PD-L2 expression on lymph node antigen presenting cells (APCs) in both male and female recipients (**Fig. 4B**). By contrast, neither PD-L1 nor PD-L2 upregulation was detected on liver APCs. Immunofluorescence of tissue sections confirmed the PD-L1 was upregulated in lymph nodes of male and female recipients with an even marked increased in males, suggesting that both non-specific inflammation and antigenic recognition may contribute to PD-1 ligands upregulation in lymph node (**Fig. S4A-B**). In particular, PD-L1 was not only upregulated on APCs but also on $CD31^+$ endothelial cells (**Fig. S4C**). To test whether the PD-1-PD-1 ligands interactions accounted for the low CTL activity detected in lymph nodes, we treated transplanted mice with a blocking anti-PD-1 antibody and then assessed killing of target cells *in vivo* (**Fig. 4C**). PD-1 blockade restored CTL killing activity in lymph nodes of male transplanted recipients. No significant increase was detected

in the liver of male mice or in lymph nodes and liver of female mice. Our results suggest that the differential induction of PD-1 ligands in distinct organs together with the upregulation of PD-1 on reactive donor T cells contributes to establishing an anatomical segregation of CTL activity during HSCT.

Donor T cells exhibit impaired sensitivity to antigen in lymph nodes due to PD-1 engagement

To further clarify how recognition of PD-1 ligands in lymph nodes may regulate T cell function locally, we visualized the behavior of MataHari T cells (and polyclonal T cells as an internal control) in lymph nodes of transplanted mice using intravital imaging (**Fig. 5A**). Interestingly, MataHari T cells exhibited the same mean velocity and straightness in male and female recipients, suggesting that, T cells did not decelerate in response to their cognate antigen in male recipients (**Fig. 5B, C, Movie S1**). To evaluate the contribution of the PD-1 pathway in this apparent lack of response to antigen, we also assessed MataHari T cell behavior in the presence of blocking anti-PD-1 antibody. PD-1 blockade promoted the arrest of MataHari T cells in male mice (**Fig. 5B, C**). No effect was noted on polyclonal T cells indicating that the arrest of donor T cells was dependent on antigen recognition. Consistent with the lack of PD-1 upregulation in control female mice, PD-1 blockade had no detectable effect on polyclonal nor on MataHari T cells in these recipients (**Fig. 5B, C, Movie S2**). We also visualized CTL ability to conjugate to male target cells in the lymph node (**Fig. 6A**). Consistent with a lack of reactivity to antigen, CTLs in male recipients failed to establish prolonged contacts with target cells (**Fig.6B-C**), but anti-PD1 treatment restored conjugate formation (**Movie S3**). As expected, CTLs in female recipients were effective in forming conjugates with target cells, irrespective of the presence of anti-PD1 mAb (**Fig. 6B-C, Movie S4**).

Altogether, our results indicate that the selective engagement of PD-1 in lymph nodes induces a local dampening of host-reactive T cells capacity to respond to antigen and to exert their killing activity during HSCT.

Anatomical segregation of CTL activity during HSCT favors site-specific tumor escape

The fact that host-reactive CTL activity can be drastically different in distinct organs of the same recipient raises the intriguing possibility that the GVL reaction may not occur efficiently in certain tissues. To test this hypothesis, we analyzed the GVL effect against a B cell lymphoma after transplantation. Male lymphoma B cells were added during the transplantation to mimic residual disease (**Fig. 7A**). In male mice transplanted with female BM but no T cells, tumors developed rapidly in both lymph nodes and liver (**Fig. 7B, C**). The addition of MataHari T cells during the transplantation led to a substantial decrease of tumor burden in the liver, indicative of an efficient GVL effect at this site. In sharp contrast, lymph nodes were heavily infiltrated with lymphoma cells as measured by flow cytometry and histology (**Fig. 7B, C**). In control female recipients, MataHari T cells were perfectly capable of controlling tumor growth in both lymph nodes and liver (**Fig. 7B, C**). Thus, miHAg-mismatched HSCT resulted in a selective defect of tumor surveillance within lymph nodes while GVL was preserved in the liver. Finally, we tested whether anti-PD-1 antibody treatment could restore tumor surveillance in lymph nodes of male recipients. To this end, we used the same experimental setting but treated mice with anti-PD-1 or an isotype control (**Fig. 7D**). We found that anti-PD-1 treatment strongly promoted tumor control in lymph nodes in male recipients (**Fig. 7E, F**). Consistently, anti-PD1 injections increased granzyme B expression of $CD8^+$ T cells in lymph nodes (**Fig. S5**). Little to no effects were detected in the liver of male recipients or in lymph nodes or liver of female recipients (**Fig. 7E, F and Fig.**

S5). Thus, anti-PD-1 blockade antagonizes the compartmentalization of CTL activity during HSCT and extends anatomical sites with efficient GVL reaction.

In sum, our results show that following allo-HSCT, the microenvironment of individual organs enforces CTL cytotoxic potential *in situ*. We propose that the spatial compartmentalization of CTL activity may not only dictate sites of GVHD, but also create niches for tumor escape.

Discussion

Allogeneic HSCT has the potential to cure hematologic malignancies, in large part through the GVL reaction mediated by host-reactive donor CTLs. Here, we report that during HSCT, CTL activity varies extensively from one organ to the other. We provide mechanistic insights into this anatomical segregation of T cell killing potential and establish a central role for differential PD-1 engagement in different tissue environments. We finally provide evidence that this compartmentalization generates spatial heterogeneity in the GVL effect and creates niches for tumor escape.

In humans, most of allo-HSCTs are HLA-matched (Gratwohl et al., 2013), and minor histocompatibility antigen mismatches are considered as a major cause for GVHD, but are also important for the GVL effect (Goulmy et al., 1996). Among miHAg, H-Y antigens have been identified as key mediators of both GVHD (Goulmy et al., 1977; Mutis et al., 1999) and GVL (Miklos et al., 2005; Nakasone et al., 2015) following female-to-male transplantations. A study in mice showed that a single H-Y antigen mismatch could induce $CD8^+$ or $CD4^+$ T cell-mediated GVHD (Toubai et al., 2012). Thus, H-Y incompatibility represents a relevant setting to study the regulation of GVHD and GVL. Using such a model in mice, we confirmed that GVHD mimicked the pattern of organ damage seen in humans, with strong infiltration of donor $CD8^+$ T cells in skin, gut and liver.

Interestingly, despite miHAg being broadly expressed in tissues, GVHD only appears in preferential target organs (Ferrara et al., 2009). Since the goal of the allo-HSCT is to promote a GVL reaction that will eliminate all residual tumor cells, it is of critical importance to clarify whether the GVL reaction is a systemic process or is instead largely restricted to specific anatomical sites, like GVHD. Anatomical heterogeneity during GVHD (and possibly GVL reaction) could originate from a differential sensitivity of host tissues to T cell-mediated

killing (Vincent et al., 2011). Although our results do not exclude this possibility, they establish that, following allo-HSCT, the CTL activity varies extensively between organs, irrespective of the target. One hypothesis to explain such a compartmentalized CTL activity could lie in the homing properties of $CD8^+$ T cells (Sackstein, 2006). In this case, highly activated T cells may preferentially home and accumulate within specific tissues such as the liver. By contrast, T cells with lower cytotoxic potential generated during HSCT may home preferentially to lymph nodes. However, CTL killing has been visualized in lymph nodes in several studies (Guarda et al., 2007; Mempel et al., 2006), suggesting that lymph nodes are not excluded from effector T cell responses in other contexts. In fact, our results do not support the idea that the compartmentalized cytotoxicity originates from preferential T cell homing. First, we showed that cytotoxic activity *in vivo* was not directly linked to CTL frequency nor to CTL:target ratio in each organ. Second, we observed that transferred $CD8^+$ T cells purified from the liver after allo-HSCT could home to lymph nodes where they lost their cytotoxic phenotype. Conversely, a substantial number of $CD8^+$ T cells purified from lymph nodes homed to the liver where they gained granzyme B expression. Thus, CTL killing potential following allo-HSCT is not a cell-intrinsic property but instead appears to be largely dictated by the tissue microenvironment.

How does the organ microenvironment regulate CTL killing potential when antigen is virtually present in each tissue? The presence of tissue-specific antigen presenting cells could potentially regulate CTL killing activity. For example, lymph node stromal cells have been shown to negatively regulate T cell responses (Tewalt et al., 2012; Dubrot et al., 2014). In the skin, the presence of Langerhans cells has been shown to increase effector cytokine production by $CD8^+$ T cells and the severity of GVHD (Bennett et al., 2011). Even in the same tissue, distinct APC populations can induce different patterns of T cell effector functions (Hufford et al., 2011; Macleod et al., 2014). Differential levels of antigen expression in

tissues may also influence GVL efficacy (Shand et al., 2014). In the liver, APCs are well known to have tolerogenic properties (Tiegs and Lohse, 2010) but can promote $CD8^+$ T cell responses in other instances (Klein and Crispe, 2006). In the specific context of allo-HSCT, we found that the contrasting CTL activity in lymph node versus liver was linked to engagement of the PD-1 pathway. Consistent with previous studies, we showed that allo-HSCT triggered PD-1 upregulation on reactive CTLs. This is very likely due to chronic antigen stimulation experienced by host-reactive CTLs. This upregulation was seen in all organs analyzed and therefore could not, by itself, account for the differential CTL activity in tissues. Strong differences were however observed in the expression of PD-1 ligands that were highly upregulated in lymph nodes but not in the liver. Interestingly, we observed that PD-1 ligands were upregulated by both hematopoietic APCs and stromal cells in lymph nodes, in accordance with the idea that organ parenchyma contributes to engage the PD-1 axis (Schilbach et al., 2007; Chaqmaqchi et al., 2013). Consistently, blockade of PD-1/PD-1-ligands interactions during allo-HSCT selectively increased CTL activity in lymph nodes.

Recent studies have shown that interference with the PD-1 pathway can globally increase the efficacy of GVL (Asakura et al., 2010; Flutter et al., 2010; Koestner et al., 2011) and severity of GVHD (Blazar et al., 2003; Saha et al., 2013). Extending these initial observations, our study indicate that the PD-1 pathway is not equally engaged in all organs, and that this mechanism contribute to establishing an anatomical hierarchy in CTL killing potential after HSCT. How the PD-1 pathway affects T cell behavior remains controversial as PD-1 blockade has been shown to promote antigen-mediated T cell stop in lymph nodes (Fife et al., 2009; Honda et al., 2014) or on the contrary to increase T cell motility (Zinselmeyer et al., 2013). Differences in the models and organs analyzed possibly accounted for these discrepancies. In our study, anti-H-Y CTLs were found to migrate vigorously in lymph nodes of male recipients without displaying obvious signs of antigen recognition. However, PD-1

blockade resulted in the deceleration and arrest of antigen-specific T cells as observed in other models (Fife et al., 2009; Honda et al., 2014). Importantly, we also observed that anti-PD-1 treatment restore the ability of CTLs to conjugate to target cells. Taken together, our results suggest that, in the specific context of allo-HSCT, elevated levels of PD-1 ligands in the lymph node microenvironment dampen T cell sensitivity to antigen and locally inhibit CTL effector functions.

Relapse is the first cause of mortality in patients with hematologic malignancies treated with allo-HSCT. We predicted that anatomical segregation of CTL activity might be reflected by an inefficient GVL reaction in tissues with the lowest killing potential resulting in the failure to clear residual disease at these sites. Accordingly, we observed that the GVL reaction controlled the growth of a B cell lymphoma in the liver but failed to do so in lymph nodes. This strongly suggests that the compartmentalization of CTL responses may create sites for tumor escape after allo-HSCT. Consistent with this idea, patients treated with allo-HSCT are more inclined to develop extramedullary relapses (including in lymph nodes) than patients treated with chemotherapy only (Harris et al., 2013; Shimizu et al., 2013). Our results highlight that anti-tumor immune responses may not be considered as anatomically uniform processes. Instead, they appear strongly modulated by individual tissue microenvironment. It will be important to identify in future studies whether such anatomical segregation is also detected in other contexts including solid tumors and metastasis.

In sum, our results establish that the PD-1 pathway contributes to spatially compartmentalize CTL activity during allo-HSCT. Organs with high and low CTL activity may be sites for GVHD or tumor escape, respectively. Recent studies have highlighted the promising efficacy of anti-PD-1 treatment in solid tumors (Armand et al., 2013; Brahmer et al., 2010; Hamid et al., 2013). Despite a possible risk in enhancing GVHD, it will be interesting to consider

whether anti-PD-1 treatment may help counteract the spatial segregation of CTL activity after allo-HSCT to ultimately suppress niches for tumor relapse.

Experimental procedures

Mice

Eight-week old wild-type C57Bl/6 (B6) mice were obtained from Charles River laboratories. *Rag1*$^{-/-}$ anti-H-Y TCR transgenic mice MataHari (Valujskikh et al., 2002), B6 transgenic mice expressing mTomato, GFP or CFP and CD11c-YFP transgenic mice were bred in our animal facility. We crossed MataHari mice with B6-ubiGFP or B6-mTomato. All animal studies were approved by the Pasteur Institute Safety Committee in accordance with French and European guidelines.

Bone Marrow Transplantation

Bone marrow was harvested from female B6 mice and T cells were depleted using CD90.2 MicroBeads Isolation kit (Miltenyi Biotec). MataHari $CD8^+$ T cells and polyclonal $CD4^+$ T cells were purified from lymph nodes and spleens of female mice using $CD8^+$ and $CD4^+$ T cell Isolation kits II (Miltenyi Biotec). Recipients were lethally irradiated with a single dose of 9 Gy delivered by an X-ray generator (RS320, Xstrahl). 4 to 6 hours after irradiation, mice were injected with $20x10^6$ T cell-depleted bone marrow cells, $5x10^6$ MataHari $CD8^+$ T cells and $5x10^6$ polyclonal $CD4^+$ T cells. GVHD was monitored two to three times a week using a previously described clinical score (including weight loss, activity, posture, skin integrity and fur texture)(Cooke et al., 1996).

Histological analysis and immunofluorescence

Perfused liver, gut, skin and lymph nodes were fixed overnight in a solution of periodate-lysine-paraformaldehyde 1%. Tissues were dehydrated in sucrose gradients and frozen in OCT compound (Tissue-Tek, Sakura Finetek). 8-μm-thick tissue sections were rehydrated

and Fc-blocked with normal mouse and rat serums in the presence of 1% Triton X100 (Sigma-Aldrich). Tissues were stained with PE- (BD Biosciences) or alexa647-conjugated (Biolegend) anti-CD8 (53-6.7) or with APC-conjugated anti-activated caspase 3 (C92-605, BD Biosciences). Sections were imaged using confocal microscope Olympus BX61WI or Leica TCS SP5. Images were processed using Fiji software (ImageJ 1.49m). To correlate activated-caspase 3 staining and $CD8^+$ T cell density, 1000x1000 μm images were divided in multiple 50x50 μm area. For each area, we quantified the mean fluorescence intensity of activated-caspase 3 and CD8 stainings.

Flow cytometry

Livers were perfused with 10mL of phosphate buffered saline (Life Technologies). Organs (lymph nodes, spleen, liver and skin) were digested in RPMI with 1mg/mL of collagenase and 0.1mg/mL of DNAse (Sigma) for 30 minutes at 37°C. Fragment of small intestine were prepared as previously described (Lochner et al., 2008). For liver and gut, cells were pelleted, resuspended in 40% isotonic Percoll solution (GE Healthcare) and underlaid with an 80% isotonic Percoll solution. Cell suspensions were Fc-blocked using anti-CD16/32 Ab (BD Pharmingen). Dead cells were labeled with Live/Dead fixable dead cell stains (Life Technologies) or Zombie Fixable Viability Kit (Biolegend). Stainings were performed using the following mAbs: CD8 (53-6.7), CD11b (M1/70), CD11c (N418), CD45 (30-F11), F4/80 (BM8), PD-1 (J43), PD-L1 (10F.9G2), PD-L2 (TY25), I-A/I-E (M5) (Biolegend). Intracellular stainings were performed using the Cytofix/Cytoperm kit (BD Biosciences) and APC-conjugated anti-Granzyme B mAb (GB11, BD Biosciences). Analyses were performed using a FACSCanto II cytometer (BD Biosciences) or an LSR/Fortessa (BD Biosciences), and analyzed using FlowJo software version 8.6.6 (TreeStar).

***In vivo* cytotoxic assay**

Male splenocytes from a B6 mouse were used as targets and female splenocytes as an internal negative control. Male and female splenocytes were labeled with Vybrant CFDA SE Cell Tracer (Life Technologies) at 1μM and 0.1μM, respectively. A 1:1 mixture of male and female splenocytes ($2x10^7$ total cells) was injected into transplanted mice at day 7. Organs were harvested 36 hours after injection of target cells. Ratios between male target ($CFSE^{high}$) and female target ($CFSE^{low}$) were calculated for each sample (R). The mean ratio measured in male recipient without effector T cells was used as a control (meanRc) to normalize samples. Killing percentage (K) was obtained with the following formula: K = 100-100*(R/meanRc). To test the effect of PD-1 blockade on *in viv*o cytotoxic activity, 250 μg of a blocking anti-PD-1 antibody (RMP1-14, Biolegend) or an IgG2Aκ isotype control (RTK2758, Biolegend) were injected intraperiteoneally on day 0, 3, 6 and 7.

Intravital imaging

Intravital two-photon imaging of popliteal lymph nodes was performed 7 days after transplantation. Mice were anesthetized, temperature was maintained at 37°C with a heating plate and popliteal lymph nodes were surgically exposed. Two-photon imaging was performed using an upright microscope DM 6000B with a SP5 confocal head (Leica Microsystems) and a 25X/1.05 NA dipping objective (Olympus). Excitation was provided by a Chameleon Ultra Ti:Sapphire laser (Coherent) tuned between 840 and 960nm. Movies were processed and analyzed with Imaris software (Bitplane) or with Fiji software (ImageJ 1.49m). The arrest coefficient was defined as the percentage of time during which instantaneous velocity was lower than 3 μm/min. Straightness was calculated as the ratio of the distance from origin to the total distance traveled. To visualize *in vivo* killing of male target cells, male splenocytes were stained with 2.5 μM Hoechst 33342 (Invitrogen), washed in PBS and then

stained with 3 μM CellTracker Orange CMRA (Life Technologies). $10x10^7$ labeled cells were injected in mice on day 7 post-transplantation. Lymph nodes were imaged 24 hours later. Target killing was measured as previously described (Mempel et al., 2006) using the Red(CMRA)/blue (Hoechst) ratio (R/B) as a read-out. To assess the effect of anti-PD-1 blockade on T cells dynamics, transplanted mice received a single intravenous injection of 250 μg of blocking anti-PD-1 antibody.

Graft versus leukemia model

A B lymphoma cell line was generated from a tumoral lymph node of a male Eμ-myc mouse (Adams et al., 1985), a transgenic mouse developing spontaneous Burkitt-like lymphomas. YFP^+ cells were obtained by retroviral transduction and sorted on a FACSAria II (BD Biosciences) and expanded in culture to establish a stable cell line. In order to test the Graft-versus-leukemia effect, male recipients were transplanted with female BM and $5x10^5$ male B lymphoma cells, with or without $5x10^6$ MataHari $CD8^+$ T cells and polyclonal $CD4^+$ T cells. Ten days after transplantation, tumor spreading was measured by flow cytometry or by confocal microscopy. Tumor cells were identified on the basis of YFP fluorescence.

Statistical analysis

All statistical tests were performed using Prism v6.0b (GraphPad). Data were expressed as mean ± SEM. We used Mann-Whitney U test for two groups comparison or Kruskal-Wallis test for multiple comparisons. One-way ANOVA test followed by Tukey's *post hoc* test was used for multiple comparisons of data with normal distribution and equal variance. All statistical tests were two-tailed with a significance level of 0.05. * $P<0.05$, ** $P<0.01$, *** $P<0.001$, ns non-significant.

Acknowledgments

The authors wish to thank Gérard Socié for insightful discussions, and members of the Bousso lab for comments on the manuscript. This work was supported by Institut Pasteur, Inserm, Ligue Contre le Cancer (Equipe Labellisée), the Fondation pour la Recherche Médicale, and an ERC starting grant (LymphocyteContacts). D.M. was supported by ITMO Cancer, Institut National du Cancer (Plan Cancer 2009-2013).

Contributions

D.M., S.C. and P.B. designed the experiments and analyzed the data. D.M., P.S., B.B., Z.G. and S.C conducted the experiments. D.M. and P.B. wrote the manuscript.

Competing financial interests

The authors declare no competing financial interest.

References

Adams, J.M., Harris, A.W., Pinkert, C.A., Corcoran, L.M., Alexander, W.S., Cory, S., Palmiter, R.D., and Brinster, R.L. (1985). The c-myc oncogene driven by immunoglobulin enhancers induces lymphoid malignancy in transgenic mice. Nature *318*, 533–538.

Armand, P., Nagler, A., Weller, E.A., Devine, S.M., Avigan, D.E., Chen, Y.-B., Kaminski, M.S., Holland, H.K., Winter, J.N., Mason, J.R., et al. (2013). Disabling immune tolerance by programmed death-1 blockade with pidilizumab after autologous hematopoietic stem-cell transplantation for diffuse large B-cell lymphoma: results of an international phase II trial. J. Clin. Oncol. Off. J. Am. Soc. Clin. Oncol. *31*, 4199–4206.

Asakura, S., Hashimoto, D., Takashima, S., Sugiyama, H., Maeda, Y., Akashi, K., Tanimoto, M., and Teshima, T. (2010). Alloantigen expression on non-hematopoietic cells reduces graft-versus-leukemia effects in mice. J. Clin. Invest. *120*, 2370–2378.

Bennett, C.L., Fallah-Arani, F., Conlan, T., Trouillet, C., Goold, H., Chorro, L., Flutter, B., Means, T.K., Geissmann, F., and Chakraverty, R. (2011). Langerhans cells regulate cutaneous injury by licensing CD8 effector cells recruited to the skin. Blood *117*, 7063–7069.

Blazar, B.R., Carreno, B.M., Panoskaltsis-Mortari, A., Carter, L., Iwai, Y., Yagita, H., Nishimura, H., and Taylor, P.A. (2003). Blockade of programmed death-1 engagement accelerates graft-versus-host disease lethality by an IFN-gamma-dependent mechanism. J. Immunol. Baltim. Md 1950 *171*, 1272–1277.

Bourgeois, C., Rocha, B., and Tanchot, C. (2002). A role for CD40 expression on CD8+ T cells in the generation of CD8+ T cell memory. Science *297*, 2060–2063.

Brahmer, J.R., Drake, C.G., Wollner, I., Powderly, J.D., Picus, J., Sharfman, W.H., Stankevich, E., Pons, A., Salay, T.M., McMiller, T.L., et al. (2010). Phase I study of single-agent anti-programmed death-1 (MDX-1106) in refractory solid tumors: safety, clinical

activity, pharmacodynamics, and immunologic correlates. J. Clin. Oncol. Off. J. Am. Soc. Clin. Oncol. *28*, 3167–3175.

Chakraverty, R. (2006). An inflammatory checkpoint regulates recruitment of graft-versus-host reactive T cells to peripheral tissues. J. Exp. Med. *203*, 2021–2031.

Chaqmaqchi, H. Al-, Sadeghi, B., Abedi-Valugerdi, M., Hashmi, S. Al-, Fares, M., Kuiper, R., Lundahl, J., Hassan, M., and Moshfegh, A. (2013). The role of programmed cell death ligand-1 (PD-L1/CD274) in the development of graft versus host disease. PloS One *8*, e60367.

Cooke, K.R., Kobzik, L., Martin, T.R., Brewer, J., Delmonte, J.J., Crawford, J.M., and Ferrara, J.L. (1996). An experimental model of idiopathic pneumonia syndrome after bone. Blood *8*, 3230–3239.

Dermime, S., Mavroudis, D., Jiang, Y.Z., Hensel, N., Molldrem, J., and Barrett, A.J. (1997). Immune escape from a graft-versus-leukemia effect may play a role in the relapse of myeloid leukemias following allogeneic bone marrow transplantation. Bone Marrow Transplant. *19*, 989–999.

Dubrot, J., Duraes, F.V., Potin, L., Capotosti, F., Brighouse, D., Suter, T., LeibundGut-Landmann, S., Garbi, N., Reith, W., Swartz, M.A., et al. (2014). Lymph node stromal cells acquire peptide-MHCII complexes from dendritic cells and induce antigen-specific $CD4^+$ T cell tolerance. J. Exp. Med. *211*, 1153–1166.

Ferrara, J.L.M., Levine, J.E., Reddy, P., and Holler, E. (2009). Graft-versus-host disease. Lancet *373*, 1550–1561.

Fife, B.T., Pauken, K.E., Eagar, T.N., Obu, T., Wu, J., Tang, Q., Azuma, M., Krummel, M.F., and Bluestone, J.A. (2009). Interactions between PD-1 and PD-L1 promote tolerance by blocking the TCR-induced stop signal. Nat. Immunol. *10*, 1185–1192.

Flies, D.B., Wang, S., Xu, H., and Chen, L. (2011). Cutting edge: A monoclonal antibody

specific for the programmed death-1 homolog prevents graft-versus-host disease in mouse models. J. Immunol. Baltim. Md 1950 *187*, 1537–1541.

Flutter, B., Edwards, N., Fallah-Arani, F., Henderson, S., Chai, J.-G., Sivakumaran, S., Ghorashian, S., Bennett, C.L., Freeman, G.J., Sykes, M., et al. (2010). Nonhematopoietic antigen blocks memory programming of alloreactive CD8+ T cells and drives their eventual exhaustion in mouse models of bone marrow transplantation. J. Clin. Invest. *120*, 3855–3868.

Goulmy, E., Termijtelen, A., Bradley, B.A., and van Rood, J.J. (1977). Y-antigen killing by T cells of women is restricted by HLA. Nature *266*, 544–545.

Goulmy, E., Schipper, R., Pool, J., Blokland, E., Falkenburg, J.H., Vossen, J., Gratwohl, A., Vogelsang, G.B., van Houwelingen, H.C., and van Rood, J.J. (1996). Mismatches of minor histocompatibility antigens between HLA-identical donors and recipients and the development of graft-versus-host disease after bone marrow transplantation. N. Engl. J. Med. *334*, 281–285.

Gratwohl, A., Baldomero, H., Gratwohl, M., Aljurf, M., Bouzas, L.F., Horowitz, M., Kodera, Y., Lipton, J., Iida, M., Pasquini, M.C., et al. (2013). Quantitative and qualitative differences in use and trends of hematopoietic stem cell transplantation: a Global Observational Study. Haematologica *98*, 1282–1290.

Guarda, G., Hons, M., Soriano, S.F., Huang, A.Y., Polley, R., Martín-Fontecha, A., Stein, J.V., Germain, R.N., Lanzavecchia, A., and Sallusto, F. (2007). L-selectin-negative CCR7-effector and memory CD8+ T cells enter reactive lymph nodes and kill dendritic cells. Nat. Immunol. *8*, 743–752.

Hamid, O., Robert, C., Daud, A., Hodi, F.S., Hwu, W.-J., Kefford, R., Wolchok, J.D., Hersey, P., Joseph, R.W., Weber, J.S., et al. (2013). Safety and tumor responses with lambrolizumab (anti-PD-1) in melanoma. N. Engl. J. Med. *369*, 134–144.

Harris, A.C., Kitko, C.L., Couriel, D.R., Braun, T.M., Choi, S.W., Magenau, J., Mineishi, S.,

Pawarode, A., Yanik, G., and Levine, J.E. (2013). Extramedullary relapse of acute myeloid leukemia following allogeneic hematopoietic stem cell transplantation: incidence, risk factors and outcomes. Haematologica *98*, 179–184.

Honda, T., Egen, J.G., Lämmermann, T., Kastenmüller, W., Torabi-Parizi, P., and Germain, R.N. (2014). Tuning of antigen sensitivity by T cell receptor-dependent negative feedback controls T cell effector function in inflamed tissues. Immunity *40*, 235–247.

Hufford, M.M., Kim, T.S., Sun, J., and Braciale, T.J. (2011). Antiviral CD8+ T cell effector activities in situ are regulated by target cell type. J. Exp. Med. *208*, 167–180.

Klein, I., and Crispe, I.N. (2006). Complete differentiation of CD8+ T cells activated locally within the transplanted liver. J. Exp. Med. *203*, 437–447.

Koestner, W., Hapke, M., Herbst, J., Klein, C., Welte, K., Fruehauf, J., Flatley, A., Vignali, D.A., Hardtke-Wolenski, M., Jaeckel, E., et al. (2011). PD-L1 blockade effectively restores strong graft-versus-leukemia effects without graft-versus-host disease after delayed adoptive transfer of T-cell receptor gene-engineered allogeneic CD8+ T cells. Blood *117*, 1030–1041.

Lochner, M., Peduto, L., Cherrier, M., Sawa, S., Langa, F., Varona, R., Riethmacher, D., Si-Tahar, M., Di Santo, J.P., and Eberl, G. (2008). In vivo equilibrium of proinflammatory IL-17+ and regulatory IL-10+ Foxp3+ RORgamma t+ T cells. J. Exp. Med. *205*, 1381–1393.

Macleod, B.L., Bedoui, S., Hor, J.L., Mueller, S.N., Russell, T.A., Hollett, N.A., Heath, W.R., Tscharke, D.C., Brooks, A.G., and Gebhardt, T. (2014). Distinct APC subtypes drive spatially segregated CD4+ and CD8+ T-cell effector activity during skin infection with HSV-1. PLoS Pathog. *10*, e1004303.

Matte-Martone, C., Venkatesan, S., Tan, H.S., Athanasiadis, I., Chang, J., Pavisic, J., and Shlomchik, W.D. (2011). Graft-versus-leukemia (GVL) against mouse blast-crisis chronic myelogenous leukemia (BC-CML) and chronic-phase chronic myelogenous leukemia (CP-CML): shared mechanisms of T cell killing, but programmed death ligands render CP-CML

and not BC-CML GVL resistant. J. Immunol. Baltim. Md 1950 *187*, 1653–1663.

Mempel, T.R., Pittet, M.J., Khazaie, K., Weninger, W., Weissleder, R., Boehmer, H. von, and Andrian, U.H. von (2006). Regulatory T cells reversibly suppress cytotoxic T cell function independent of effector differentiation. Immunity *25*, 129–141.

Miklos, D.B., Kim, H.T., Miller, K.H., Guo, L., Zorn, E., Lee, S.J., Hochberg, E.P., Wu, C.J., Alyea, E.P., Cutler, C., et al. (2005). Antibody responses to H-Y minor histocompatibility antigens correlate with chronic graft-versus-host disease and disease remission. Blood *105*, 2973–2978.

Mutis, T., Gillespie, G., Schrama, E., Falkenburg, J.H., Moss, P., and Goulmy, E. (1999). Tetrameric HLA class I-minor histocompatibility antigen peptide complexes demonstrate minor histocompatibility antigen-specific cytotoxic T lymphocytes in patients with graft-versus-host disease. Nat. Med. *5*, 839–842.

Nakasone, H., Tian, L., Sahaf, B., Kawase, T., Schoenrock, K., Perloff, S., Ryan, C.E., Paul, J., Popli, R., Wu, F., et al. (2015). Allogeneic HY antibodies detected 3 months after female to male sex-mismatched HCT predict chronic GVHD and non-relapse mortality. Blood.

Norde, W.J., Maas, F., Hobo, W., Korman, A., Quigley, M., Kester, M.G.D., Hebeda, K., Falkenburg, J.H.F., Schaap, N., de Witte, T.M., et al. (2011). PD-1/PD-L1 interactions contribute to functional T-cell impairment in patients who relapse with cancer after allogeneic stem cell transplantation. Cancer Res. *71*, 5111–5122.

Pasquini, M., Wang, Z., Horowitz, M.M., and Gale, R.P. (2013). 2013 report from the Center for International Blood and Marrow Transplant Research (CIBMTR): current uses and outcomes of hematopoietic cell transplants for blood and bone marrow disorders. Clin. Transpl. 187–197.

Sackstein, R. (2006). A revision of Billingham's tenets: the central role of lymphocyte migration in acute graft-versus-host disease. Biol. Blood Marrow Transplant. J. Am. Soc.

Blood Marrow Transplant. *12*, 2–8.

Saha, A., Aoyama, K., Taylor, P.A., Koehn, B.H., Veenstra, R.G., Panoskaltsis-Mortari, A., Munn, D.H., Murphy, W.J., Azuma, M., Yagita, H., et al. (2013). Host programmed death ligand 1 is dominant over programmed death ligand 2 expression in regulating graft-versus-host disease lethality. Blood *122*, 3062–3073.

Schilbach, K., Schick, J., Wehrmann, M., Wollny, G., Simon, P., Perikles, S., Schlegel, P.G., and Eyrich, M. (2007). PD-1-PD-L1 pathway is involved in suppressing alloreactivity of heart infiltrating t cells during murine gvhd across minor histocompatibility antigen barriers. Transplantation *84*, 214–222.

Schneidawind, D., Pierini, A., and Negrin, R.S. (2013). Regulatory T cells and natural killer T cells for modulation of GVHD following allogeneic hematopoietic cell transplantation. Blood *122*, 3116–3121.

Sega, E.I., Leveson-Gower, D.B., Florek, M., Schneidawind, D., Luong, R.H., and Negrin, R.S. (2014). Role of lymphocyte activation gene-3 (Lag-3) in conventional and regulatory T cell function in allogeneic transplantation. PloS One *9*, e86551.

Shand, J.C., Qin, H., Nasholm, N., Capitini, C.M., and Fry, T.J. (2014). Minor antigen distribution predicts site-specific graft-versus-tumor activity of adoptively transferred, minor antigen-specific CD8 T Cells. Biol. Blood Marrow Transplant. J. Am. Soc. Blood Marrow Transplant. *20*, 26–36.

Shimizu, H., Saitoh, T., Hatsumi, N., Takada, S., Handa, H., Jimbo, T., Sakura, T., Miyawaki, S., and Nojima, Y. (2013). Prevalence of extramedullary relapses is higher after allogeneic stem cell transplantation than after chemotherapy in adult patients with acute myeloid leukemia. Leuk. Res. *37*, 1477–1481.

Tewalt, E.F., Cohen, J.N., Rouhani, S.J., Guidi, C.J., Qiao, H., Fahl, S.P., Conaway, M.R., Bender, T.P., Tung, K.S., Vella, A.T., et al. (2012). Lymphatic endothelial cells induce

tolerance via PD-L1 and lack of costimulation leading to high-level PD-1 expression on CD8 T cells. Blood *120*, 4772–4782.

Tiegs, G., and Lohse, A.W. (2010). Immune tolerance: what is unique about the liver. J. Autoimmun. *34*, 1–6.

Toubai, T., Tawara, I., Sun, Y., Liu, C., Nieves, E., Evers, R., Friedman, T., Korngold, R., and Reddy, P. (2012). Induction of acute GVHD by sex-mismatched H-Y antigens in the absence of functional radiosensitive host hematopoietic-derived antigen-presenting cells. Blood *119*, 3844–3853.

Valujskikh, A., Lantz, O., Celli, S., Matzinger, P., and Heeger, P.S. (2002). Cross-primed CD8(+) T cells mediate graft rejection via a distinct effector pathway. Nat. Immunol. *3*, 844–851.

Veenstra, R.G., Taylor, P.A., Zhou, Q., Panoskaltsis-Mortari, A., Hirashima, M., Flynn, R., Liu, D., Anderson, A.C., Strom, T.B., Kuchroo, V.K., et al. (2012). Contrasting acute graft-versus-host disease effects of Tim-3/galectin-9 pathway blockade dependent upon the presence of donor regulatory T cells. Blood *120*, 682–690.

Vincent, K., Roy, D.-C., and Perreault, C. (2011). Next-generation leukemia immunotherapy. Blood *118*, 2951–2959.

Wilhelm, K., Ganesan, J., Müller, T., Dürr, C., Grimm, M., Beilhack, A., Krempl, C.D., Sorichter, S., Gerlach, U.V., Jüttner, E., et al. (2010). Graft-versus-host disease is enhanced by extracellular ATP activating P2X7R. Nat. Med. *16*, 1434–1438.

Zinselmeyer, B.H., Heydari, S., Sacristán, C., Nayak, D., Cammer, M., Herz, J., Cheng, X., Davis, S.J., Dustin, M.L., and McGavern, D.B. (2013). PD-1 promotes immune exhaustion by inducing antiviral T cell motility paralysis. J. Exp. Med. *210*, 757–774.

Figure legends

Figure 1: HSCT transplantation with H-Y mismatch induces GVHD

(**A**) Male or female recipients mice were lethally irradiated and transplanted with $20x10^6$ T cell-depleted bone marrow cells, $5x10^6$ MataHari $CD8^+$ T cells and $5x10^6$ polyclonal $CD4^+$ T cells. (**B**) Male recipients developed GVHD from day 7 after transplantation. Clinical scores of GVHD over time for the indicated transplantation group. Data are pooled from five independent experiments. (**C**) Confocal microscopy of liver, gut and skin showed infiltration by MataHari $CD8^+$ T cells (yellow) in male recipients (day 7) but not in female controls (scale bar: 200 μm). (**D**) GVHD lesions in liver of male recipients were identified by staining for activated-caspase 3 staining (blue). Representative images showing apoptotic cells in male recipients but not in female controls (scale bar: 50 μm). (**E**) To relate cell apoptosis to CTL density, images were divided in multiple areas of 50x50 μm. Mean fluorescence of activated-caspase 3 staining was measured together with CD8 staining intensity, as an indicator of MataHari $CD8^+$ T cells density. In the liver of male recipients, activated-caspase 3 staining was correlated with MataHari $CD8^+$ T cell density ($r=0.8983$, Pearson correlation coefficient). Data are representative of two independent experiments with 3 to 4 mice per group in each experiment. See also Figure S1.

Figure 2: Spatial compartmentalization of CTL activity during allo-HSCT

(**A**) Male or control female recipients were transplanted with female bone marrow cells, MataHari $CD8^+$ T cells and polyclonal $CD4^+$ T cells. Male recipients transplanted with T cell-depleted bone marrow only were used as negative controls. Seven days after transplantation, a mixture of male ($CFSE^{high}$) and female (negative control, $CFSE^{low}$) splenocytes were injected intravenously. (**B**) After 36 hours, $CFSE^{high}/CFSE^{low}$ ratios were measured in the indicated

organs and are shown in representative FACS histograms. Killing percentage was calculated in each organ. Data are pooled from 3 independent experiments with 6 to 11 mice per group. (**C**) To visualize killing *in vivo*, recipients were transplanted with GFP-expressing MataHari $CD8^+$ T cells. Seven days after transplantation, male targets were labeled with CMRA (red) and Hoechst33342 (blue) and the red/blue ratio (R/B) was used as a read-out of cell viability. (**D**) Popliteal lymph nodes were imaged 24 hours after target transfer to visualize live (high R/B ratio, appearing in red) and dead (low R/B ratio, appearing in magenta) targets. White circles indicate dead targets. (**E**) The graph shows the mean velocity of each target relative to its mean R/B ratio. For each group, data are representative of >10 movies obtained from 4 mice. See also Figure S2.

Figure 3: CTL killing phenotype is acquired in specific tissue microenvironments

(**A**) Granzyme B expression in MataHari $CD8^+$ T cells was measured by intracellular staining on day 7 after transplantation in the indicated organs. Data are pooled from 3 independent experiments. (**B**) Two groups of male recipients were transplanted with GFP- or mTomato-expressing MataHari $CD8^+$ T cells. One week after transplantation, MataHari-GFP or MataHari-mTomato $CD8^+$ T cells were harvested from lymph nodes and liver. A 1:1 mixture of MataHari $CD8^+$ T cells from LN and liver (distinguished by the expression of different fluorescent proteins) was injected into male recipients transplanted 7 days previously with colorless MataHari $CD8^+$ T cells. Two days after transfer, granzyme B expression was measured by flow cytometry in GFP^+ and $mTomato^+$ MataHari $CD8^+$ T cells. (**C**). Representative FACS histograms show granzyme B expression in MataHari $CD8^+$ T cell subsets isolated from lymph nodes and liver before and after the transfer (**D**) Graph compiling granzyme B expression on MataHari T cells recovered from lymph nodes, spleen, bone-marrow, liver and gut after adoptive transfer. Note that MataHari $CD8^+$ T cells acquired

organ-specific granzyme B expression irrespective of the location from where they had been initially isolated. Data are pooled from 2 independent experiments. See also Figure S3.

Figure 4: The PD-1 axis selectively impairs CTL activity in lymph nodes after allo-HSCT

(**A**) High PD-1 expression by T cells in H-Y mismatched HSCT. PD-1 expression was analyzed in MataHari $CD8^+$ T cells isolated from the indicated organs 7 days after transplantation in male recipients or female controls. Data are pooled from 4 independent experiments. (**B**) PD-L1 and PD-L2 expression were quantified by flow cytometry on macrophages ($CD11b^+$ $F4/80^+$) and dendritic cells ($CD11c^+$ $MHCII^{high}$) in lymph nodes and liver of the indicated groups. PD-L1 and PD-L2 expression were significantly increased on macrophages and dendritic cells in lymph nodes but not in the liver. Data are representative of four independent experiments. (**C**) Transplanted mice received repeated injections of blocking anti-PD-1 antibody (or isotype control) on day 0, 3 and 6 after HSCT. On day 7, *in vivo* cytotoxic activity of MataHari $CD8^+$ T cells was assessed as described in Fig. 2A. Note that, in male recipients, PD-1 blockade restored cytotoxic activity in lymph nodes. Data are representative of two independent experiments with 3 to 6 mice per group and per experiment. See also Figure S4.

Figure 5: PD-1 blockade restores CTL sensitivity to antigen in lymph nodes

(**A**) Recipients were transplanted with female bone marrow, MataHari $CD8^+$ T cells (10% of GFP-expressing and 90% colorless T cells), CFP^+ polyclonal $CD8^+$ T cells and colorless polyclonal $CD4^+$ T cells. On day 7 post-transplantation, mice received a single dose of either blocking anti-PD-1 antibody or an isotype control. Two-photon imaging of popliteal lymph nodes was performed 18 hours after injection. (**B**) Trajectories of MataHari $CD8^+$ T cells in

female controls or in male recipients, treated or not with anti-PD-1 antibody. For each condition, 20 tracks over 15 minutes are shown. Tick intervals, 20 μm. Data are representative of two independent experiments with 4 to 5 mice per group and per experiment. (**C**) Graphs compiling the mean velocity, straightness coefficient and arrest coefficient of polyclonal (blue) or MataHari (black) $CD8^+$ T cells in male or female recipients and in the presence or absence of anti-PD-1 antibody. Of note, due to the high expansion of MataHari T cells in male recipients, polyclonal $CD8^+$ T cells were scarce as compared to female controls. For each condition, data are pooled from 3 representative movies performed in two independent experiments. See also Movie S1 and S2.

Figure 6: PD-1 blockade restores CTL conjugation to target cells in lymph nodes

(**A**) Recipients were transplanted with female bone marrow, MataHari $CD8^+$ T cells (10% of GFP-expressing and 90% colorless T cells), and colorless polyclonal $CD4^+$ T cells. On day 7 post-transplantation, mice received a single dose of either blocking anti-PD-1 antibody or an isotype control. CFP-expressing male splenocytes were injected 6h later. Two-photon imaging of popliteal lymph nodes was performed 12 hours after target cell injection. (**B**) Representative images illustrating the CTL-target cell interactions in male or female recipients in the presence or absence of anti-PD1. (**C**) Quantification of the frequency of target cells establishing contacts (>2.5 min) with CTLs. Each dot represent the mean value obtained in an individual movie. See also Movie S3 and S4.

Figure 7: Tumor relapses are enhanced in lymph nodes after allo-HSCT

(**A**) Recipients were transplanted with female bone marrow and B lymphoma cells (YFP^+) in the presence or absence of MataHari $CD8^+$ T cells and polyclonal $CD4^+$ T cells. Tumor infiltration was monitored by flow cytometry and confocal microscopy 10 days after

transplantation. (**B**) FACS profiles show the percentage of tumor cells in the indicated organs for each transplantation group. (**C**) Confocal immunofluorescence on frozen lymph node or liver sections showing the extent of lymphoma B cell infiltration and $CD8^+$ T cells in male and female recipients. Scale bar, 200 μm. Data are pooled from two independent experiments with 2 to 4 mice per group and per experiment. (**D**) Recipients were transplanted with female bone marrow and B lymphoma cells (YFP^+) in the presence or absence of MataHari $CD8^+$ T cells and polyclonal $CD4^+$ T cells. Mice were treated on the indicated days with anti-PD-1 or an isotype control. (**E**) FACS profiles show the percentage of tumor cells in the indicated organs for each transplantation group. (**F**) The number of tumor cells recovered in the indicated organs is shown for each transplantation and treatment group. Results are pooled from 2 independent experiments (7 mice per group). See also Figure S7.

Michonneau et al., figure 1

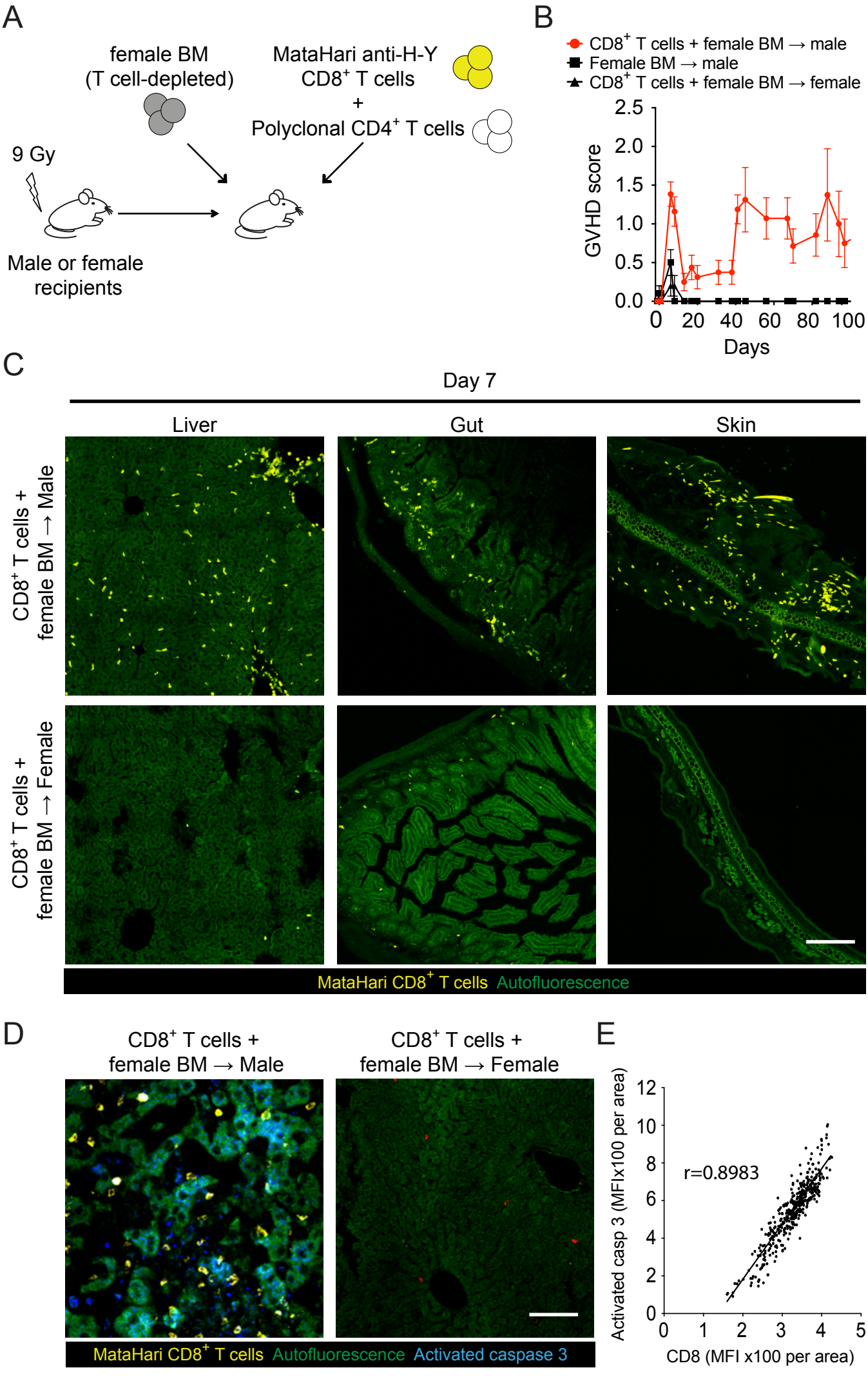

Michonneau et al., figure 2

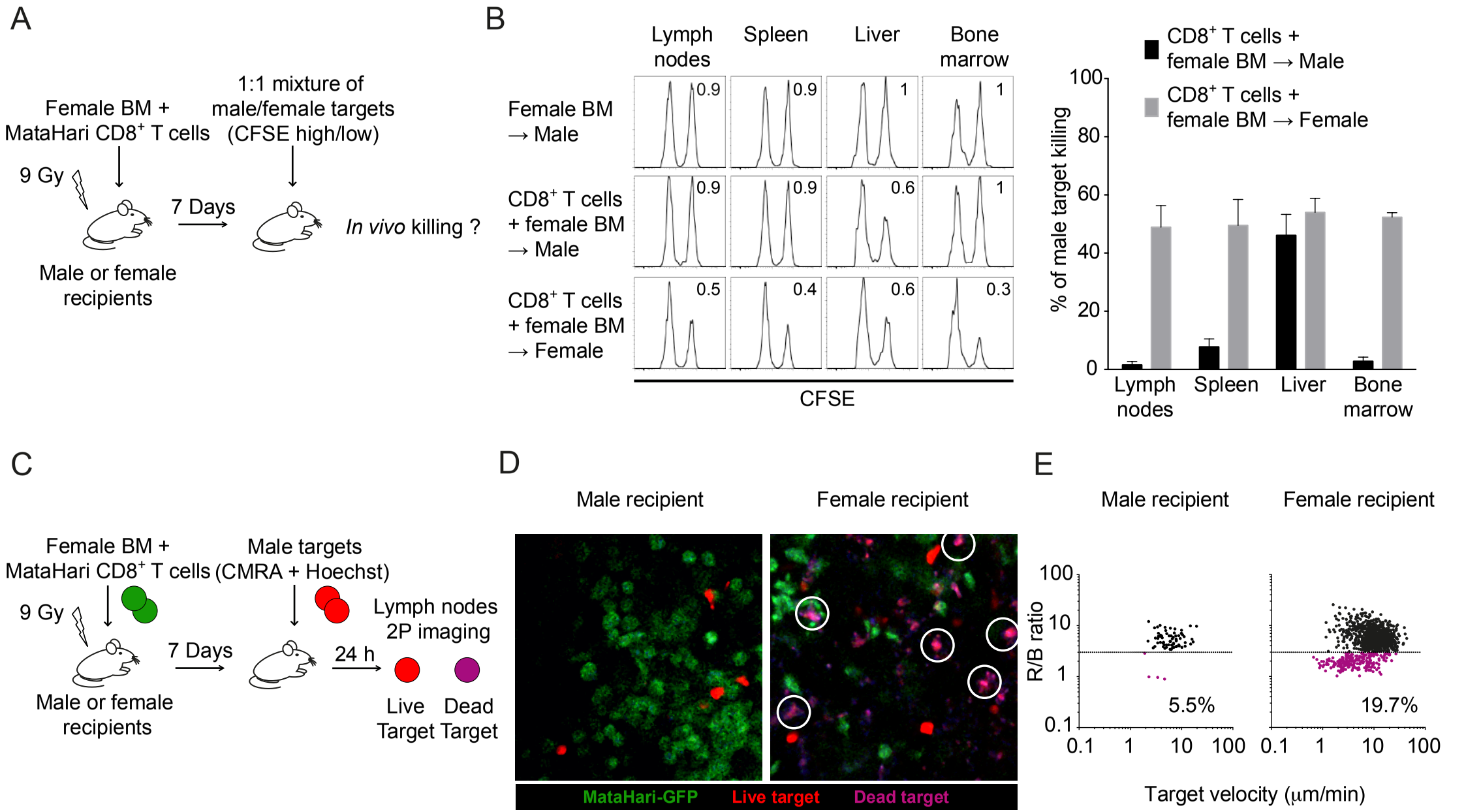

Michonneau et al., figure 3

A

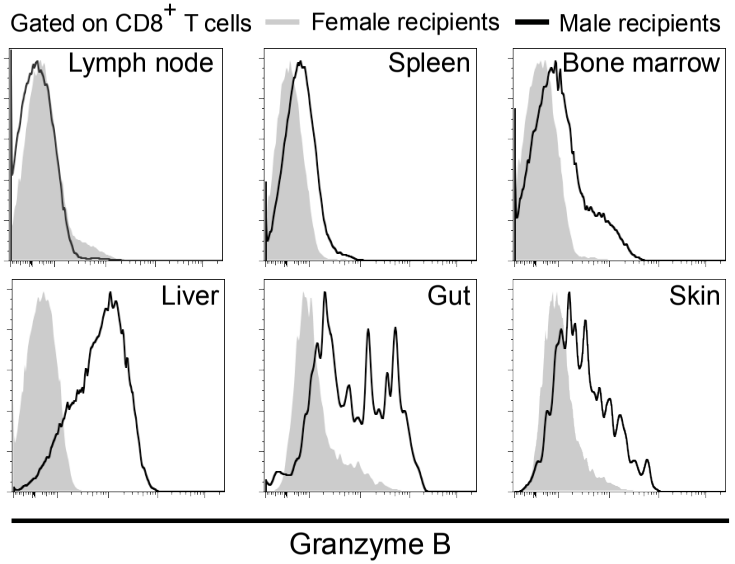

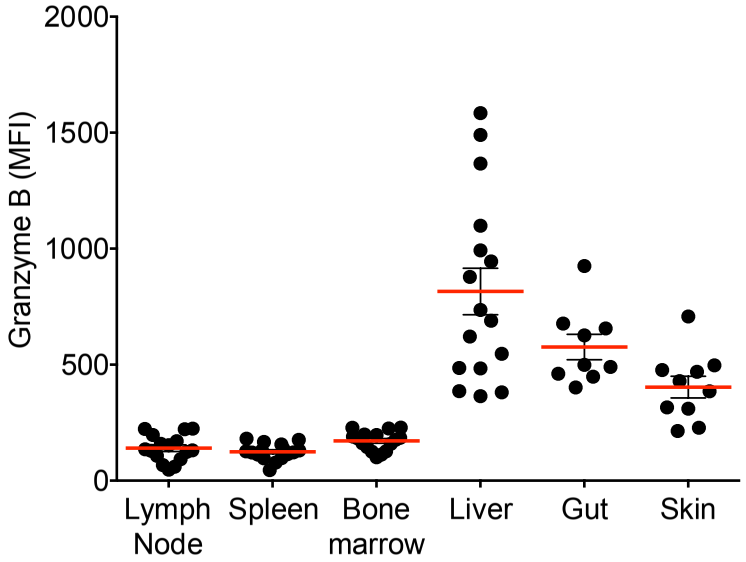

B

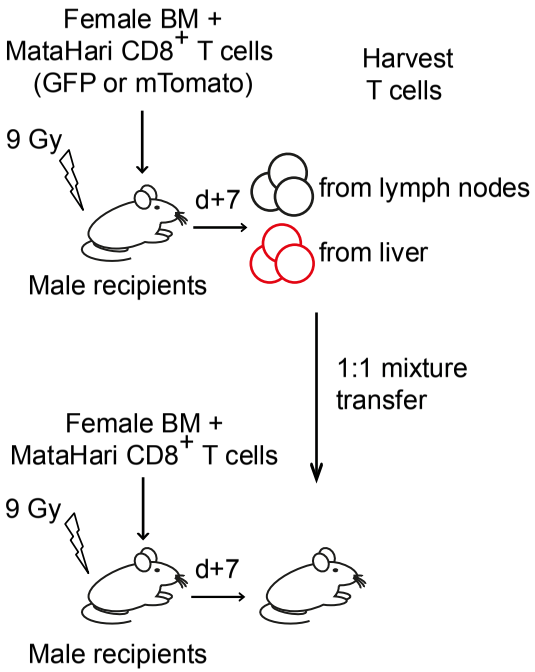

C

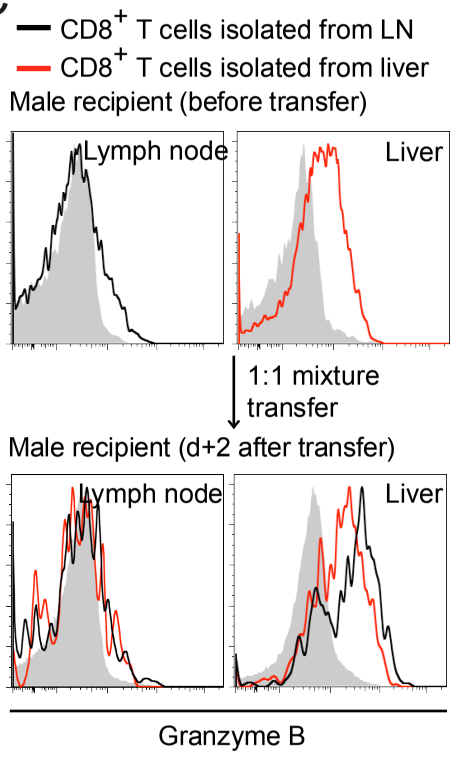

D

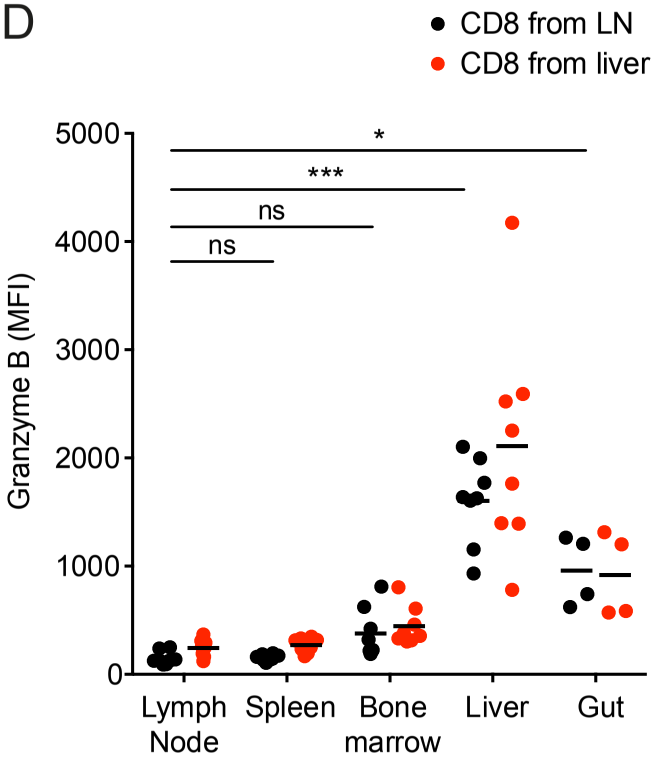

Michonneau et al., figure 4

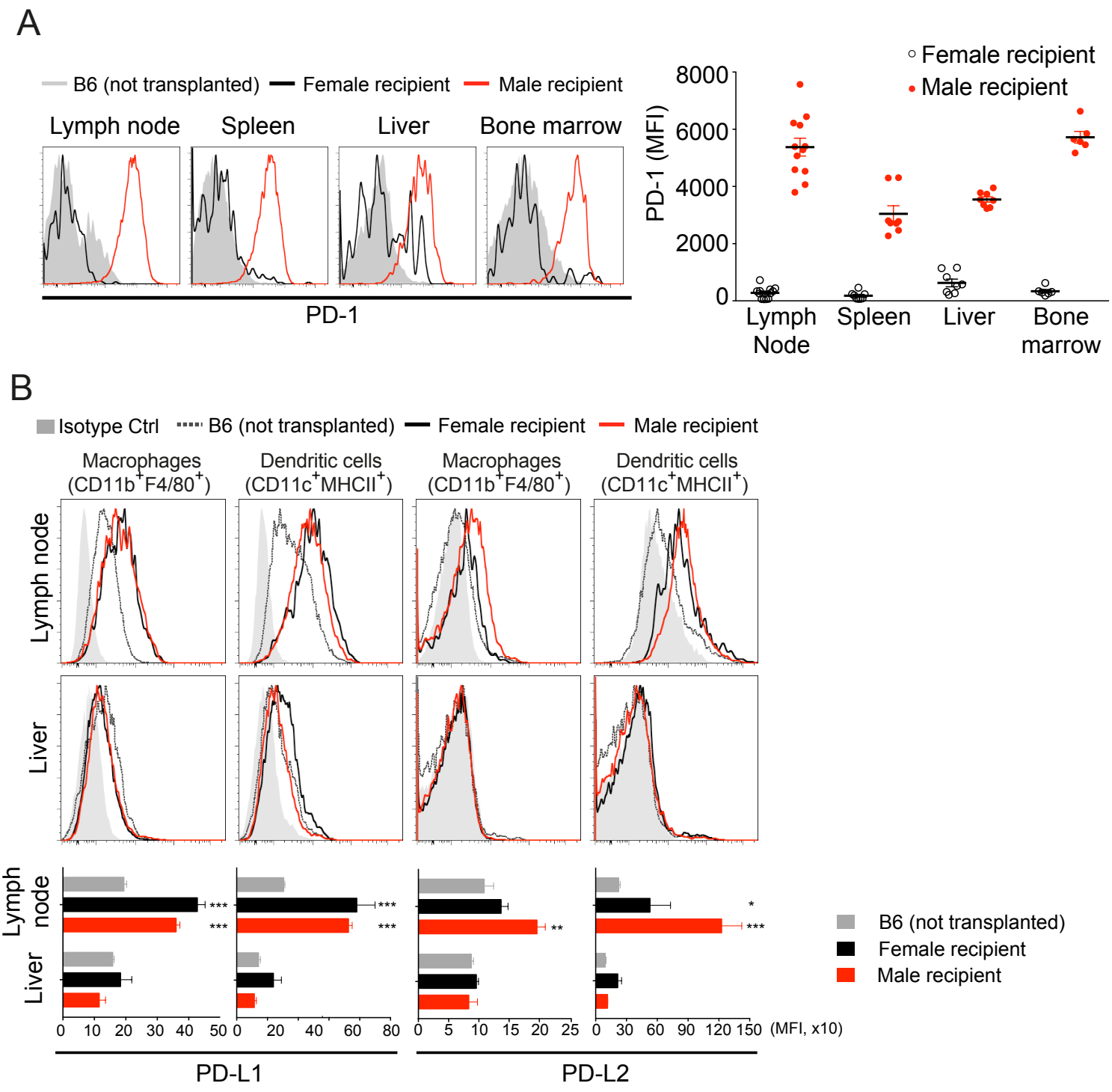

Michonneau et al., figure 5

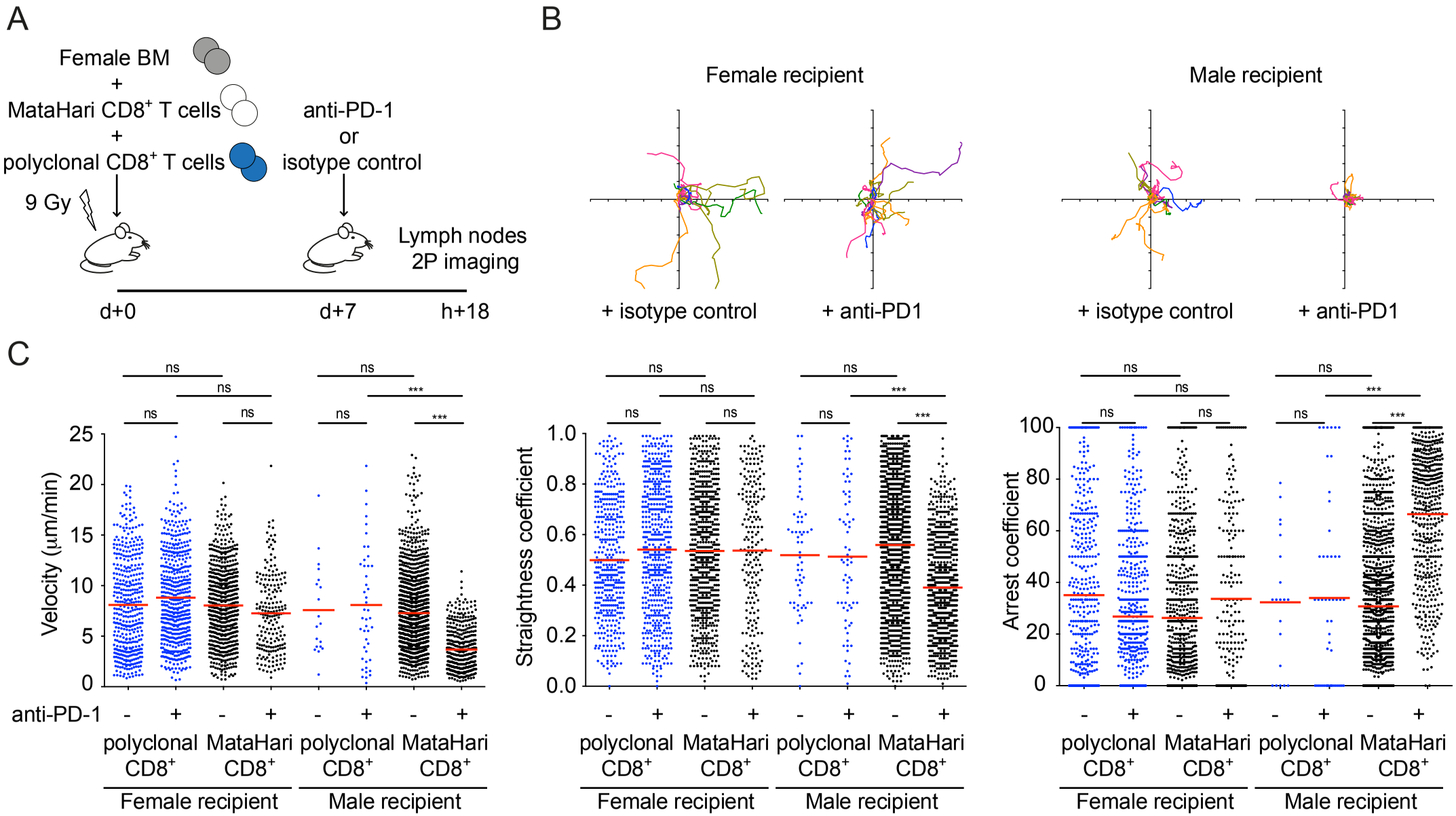

Michonneau et al., figure 6

A

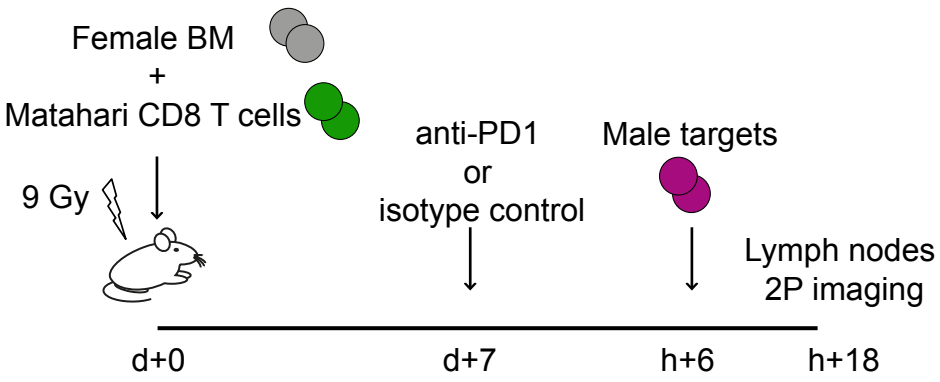

B

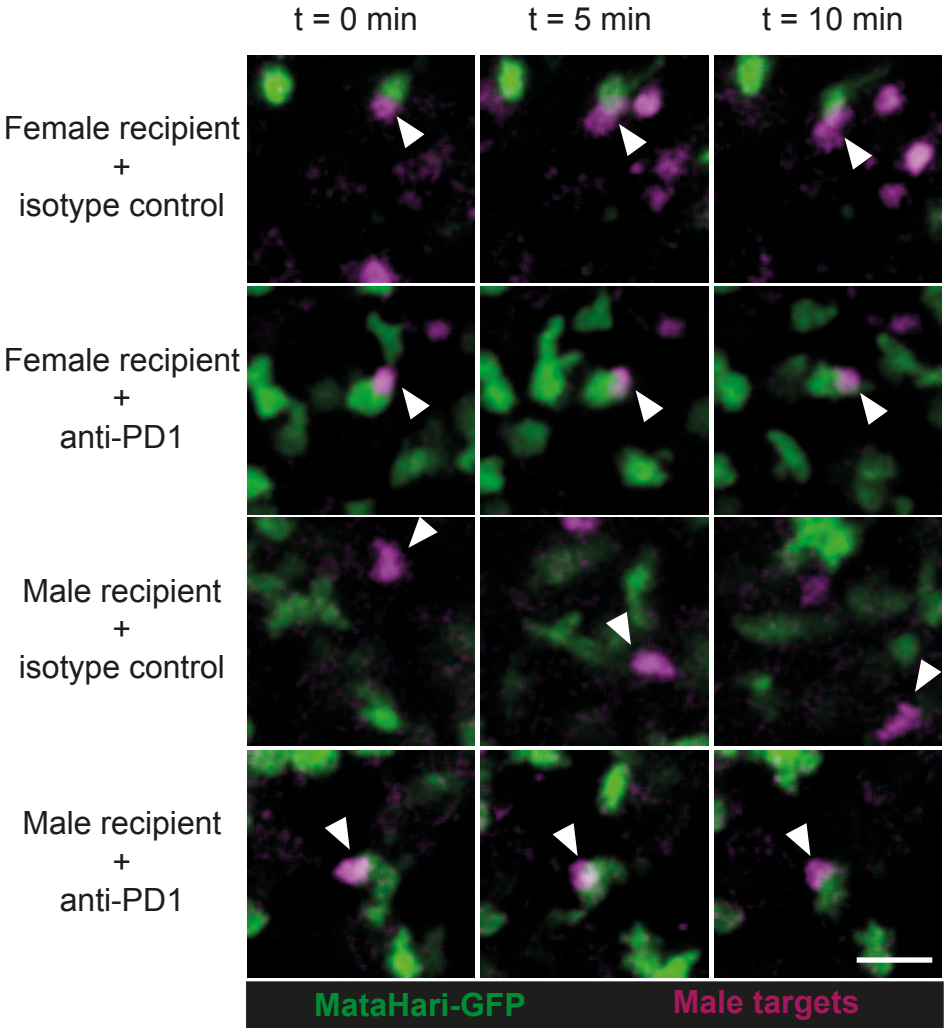

C

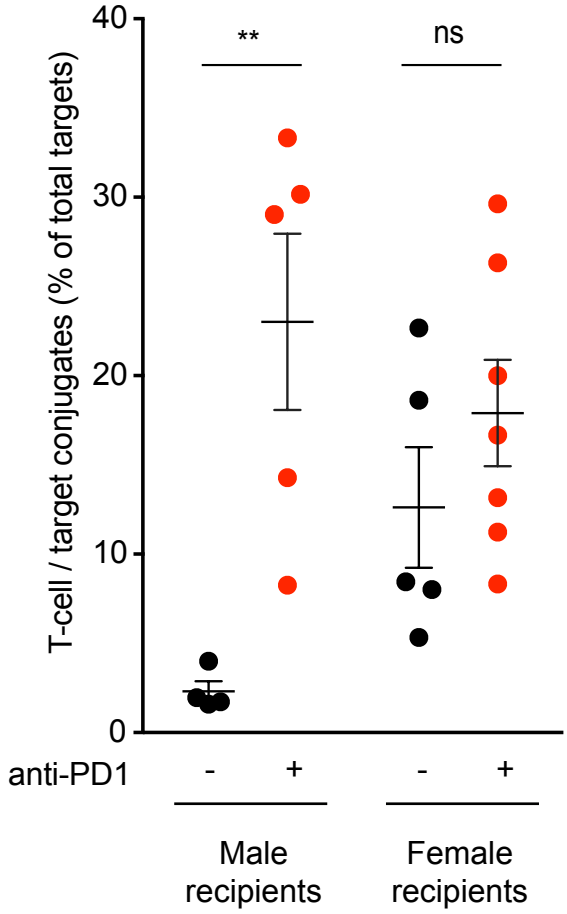

Michonneau et al., figure 7

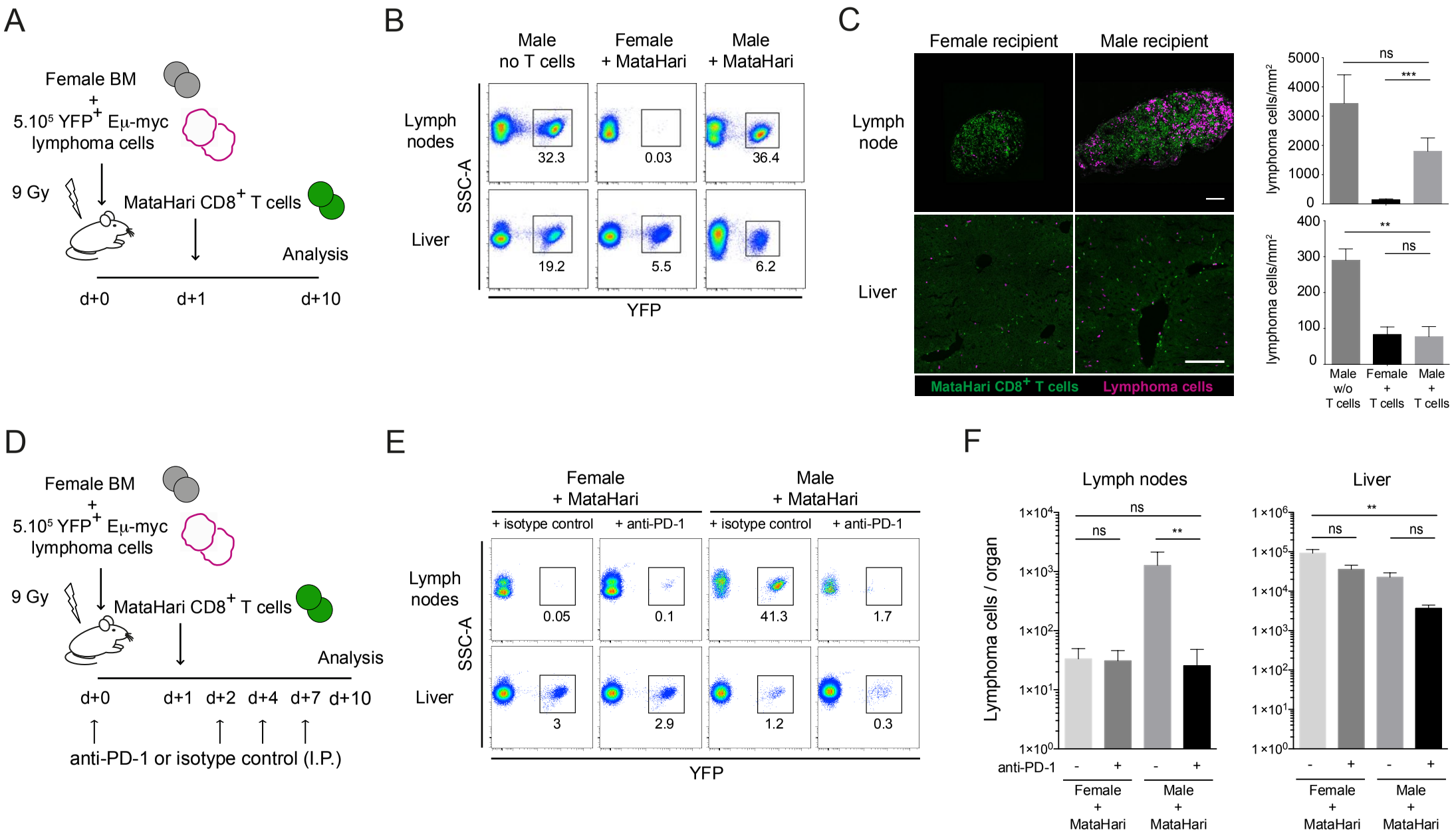

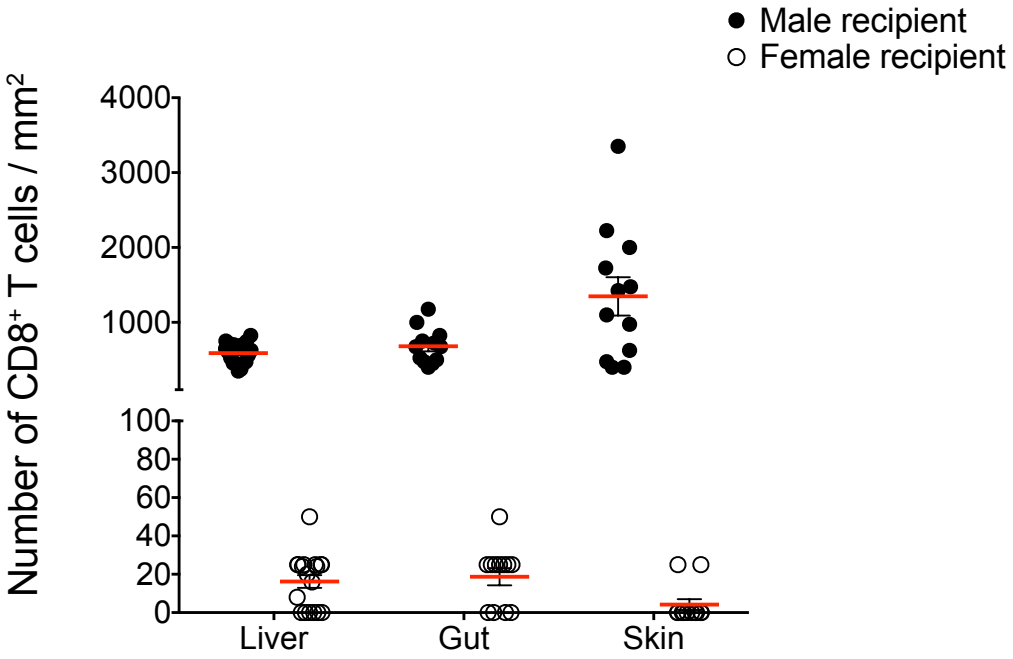

Figure S1, related to Figure 1: Donor T cells infiltrates classical GVHD target organs in a model of HY-mismatched HSCT.

Male or female recipients mice were lethally irradiated and transplanted with $20x10^6$ T cell-depleted bone marrow cells, $5x10^6$ MataHari $CD8^+$ T cells and $5x10^6$ polyclonal $CD4^+$ T cells. On day 7, the density of $CD8^+$ T cells was measured in the indicated organs using confocal imaging of frozen tissue sections.

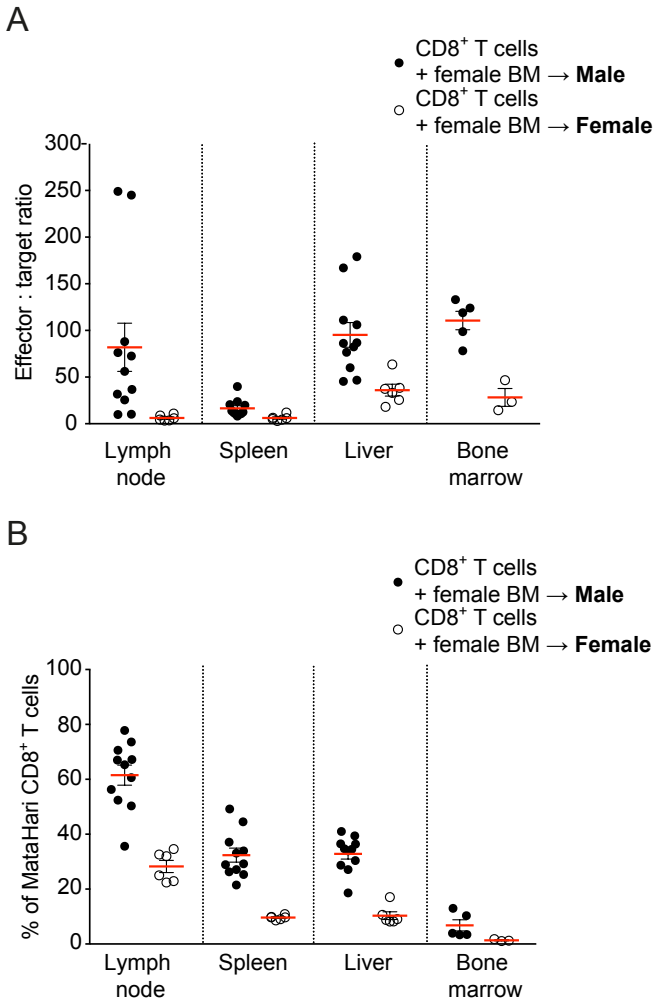

Figure S2, related to Figure 2: Compartmentalized CTL activity cannot be accounted for by differences in effector:target ratio nor in donor T cell frequency between organs.

Male or control female recipients were transplanted with female bone marrow cells, MataHari $CD8^+$ T cells and polyclonal $CD4^+$ T cells. Seven days after transplantation, a mixture of male ($CFSE^{high}$) and female (negative control, $CFSE^{low}$) splenocytes were injected intravenously. (**A**) After 36 hours, local effector:target ratios were estimated by dividing the number of MataHari $CD8^+$ T cells by the number of female splenocytes ($CFSE^{low}$). (**B**) Frequencies of MataHari $CD8^+$ T cells (among $CD45^+$ cells) were determined in the indicated organs 36 hours after targets injection. Results are pooled from 3 independent experiments.

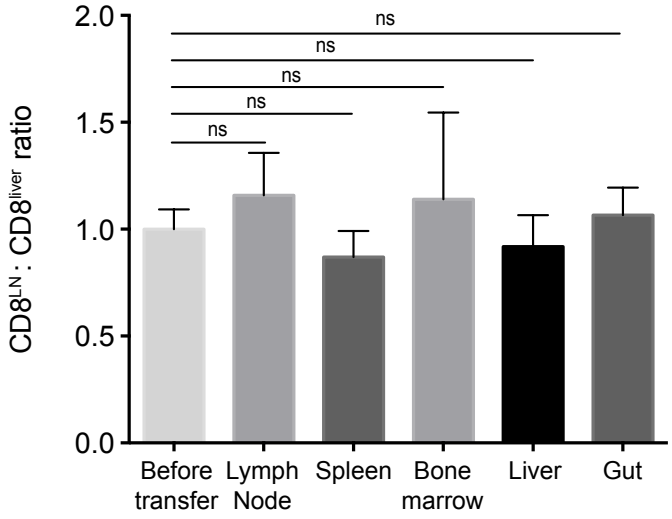

Figure S3, related to Figure 3: Similar homing properties of CTLs purified from lymph nodes and liver after adoptive transfer.

Two groups of male recipients were transplanted with GFP- or mTomato-expressing MataHari $CD8^+$ T cells, respectively. One week after transplantation, MataHari-GFP or MataHari-mTomato $CD8^+$ T cells were harvested from lymph nodes and liver. A 1:1 mixture of MataHari $CD8^+$ T cells from LN and liver (distinguished by the expression of different fluorescent proteins, referred to as $CD8^{LN}$ and $CD8^{liver}$, respectively) was injected into male recipients transplanted 7 days previously with female bone marrow and non-fluorescent MataHari $CD8^+$ T cells. Two days after adoptive transfer, the ratio of the two transferred T cell populations was measured in lymph nodes, spleen, bone marrow, liver and gut of the second recipient. Note that the T cell ratio before transfer was similar to those measured after transfer in all organs tested (ns, non significant with Kruskal-Wallis test).

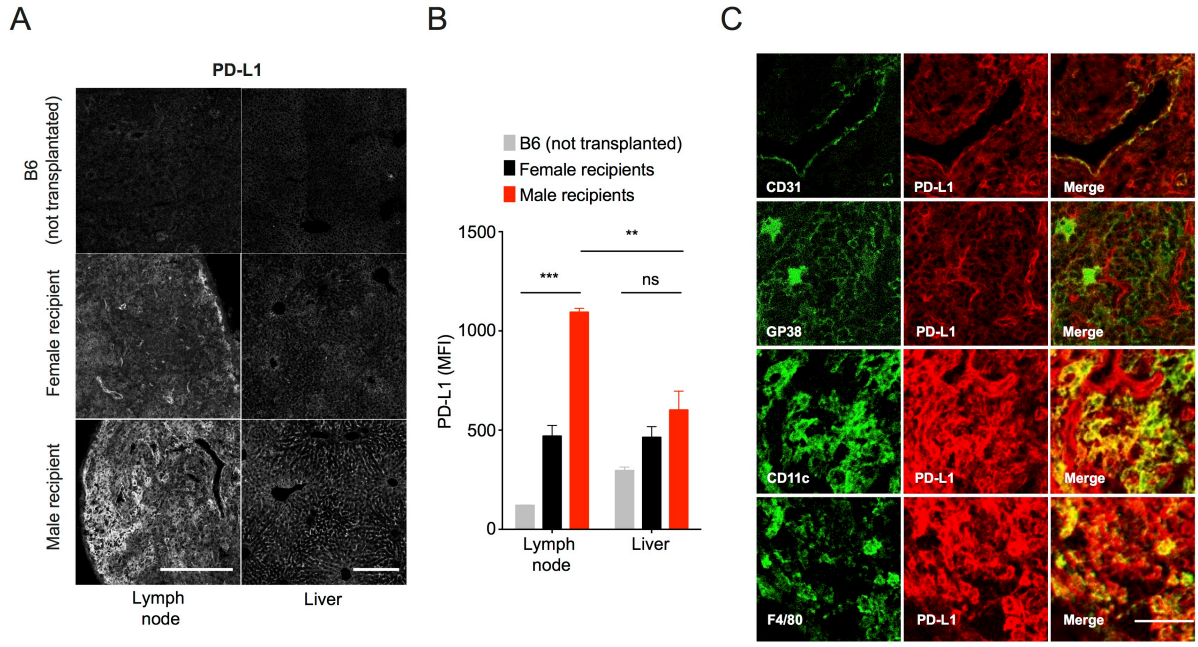

Figure S4, related to Figure 4: PD-L1 is overexpressed in lymph nodes after allo-HSCT.

Male or female recipients were lethally irradiated and transplanted with T cell-depleted bone marrow cells, MataHari $CD8^+$ T cells and polyclonal $CD4^+$ T cells. (**A**) On day 7, PD-L1 expression was measured in lymph nodes and liver using immunofluorescence staining of frozen tissue sections. Non-transplanted B6 mice were used as reference for basal expression. Scale bar, 200 µm. (**B**) Mean intensity of PD-L1 staining was calculated from confocal images. ** $P<0.01$, *** $P<0.001$, ns non-significant, with Mann-Whitney test. (**C**) PD-L1 expression was measured in lymph nodes in conjunction with F4/80, CD11c, gp38 and CD31. Note that PD-L1 was upregulated on $CD11c^+$, $F4/80^+$ and $CD31^+$ cells but not on $gp38^+$ stromal cells. Scale bar, 50 µm.

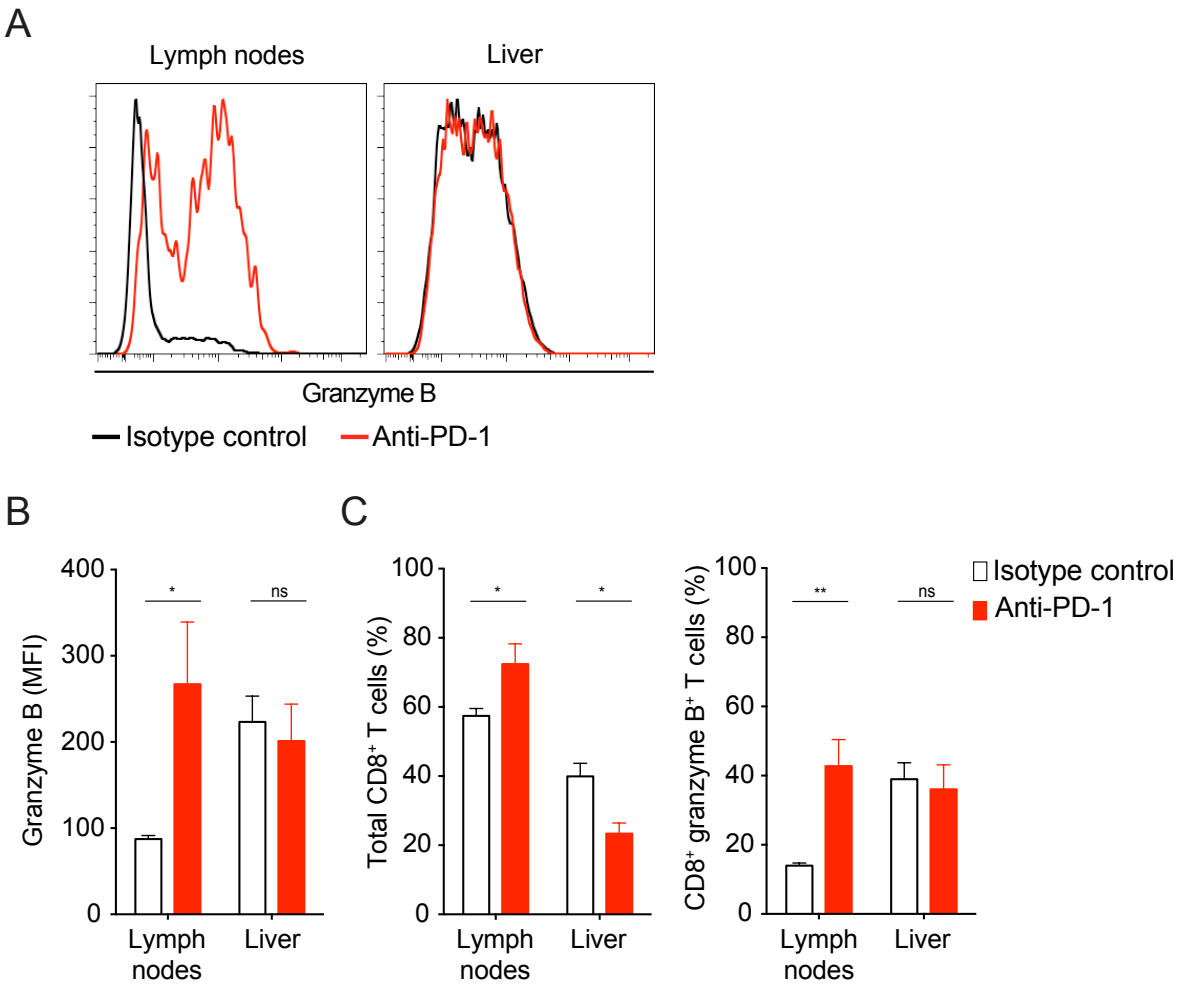

Figure S5, related to Figure 7: Anti-PD-1 treatment restore granzyme B expression on lymph node CD8$^+$ T cells.

(**A-C**) Male or female recipients were transplanted with female bone marrow and B lymphoma cells (YFP$^+$) in the presence or absence of MataHari CD8$^+$ T cells and polyclonal CD4$^+$ T cells. Mice were treated with anti-PD-1 or an isotype control as described in the legend of Fig. 6. On day 10, intracellular granzyme B content was assessed in CD8+ T cells isolated from the indicated organs using flow cytometry.

Movie legends

Movie S1, related to Figure 5. Anti-PD-1 treatment promotes T cell arrest in lymph nodes during allo-HSCT

Male recipients were transplanted with bone marrow from female CD11c-YFP mice, MataHari $CD8^+$ T cells (10% of GFP-expressing and 90% non-fluorescent T cells), CFP^+ polyclonal $CD8^+$ T cells and colorless polyclonal $CD4^+$ T cells. On day 7 post-transplantation, mice received a single dose of blocking anti-PD-1 antibody or of an isotype control. Two-photon imaging of popliteal lymph nodes was performed 18 hours after injection. MataHari T cells are shown in cyan, donor DCs (CD11c-YFP reporter positive) in yellow. Circles indicate arrested T cells. Due to the high expansion of MataHari T cells in male recipients, polyclonal (CFP^+) $CD8^+$ T cells were rare in these movies. Scale bar, 20 μm. Representative of >15 movies obtained in 4-5 mice per group.

Movie S2, related to Figure 5. Anti-PD-1 treatment has no detectable effect on T cell dynamics in syngeneic HSCT

Female recipients were transplanted with bone marrow from female CD11c-YFP mice, MataHari $CD8^+$ T cells (10% of GFP-expressing and 90% non-fluorescent T cells), CFP^+ polyclonal $CD8^+$ T cells and colorless polyclonal $CD4^+$ T cells. On day 7 post-transplantation, mice received a single dose of blocking anti-PD-1 antibody or of an isotype control. Two-photon imaging of popliteal lymph nodes was performed 18 hours after injection. MataHari T cells are shown in cyan, polyclonal $CD8^+$ T cells in blue, donor DCs (CD11c-YFP reporter positive) in yellow. Scale bar, 20 μm. Representative of >15 movies obtained in 4 mice per group.

Movie S3, related to Figure 6. Anti-PD-1 treatment promotes T cell-target cell interactions in lymph nodes during allo-HSCT

Male recipients were transplanted with female bone marrow, MataHari CD8+ T cells (10% of GFP-expressing and 90% colorless T cells), and colorless polyclonal CD4+ T cells. On day 7 post-transplantation, mice received a single dose of either blocking anti-PD-1 antibody or an isotype control. CFP-expressing male splenocytes were injected 6h later. Two-photon imaging of popliteal lymph nodes was performed 12 hours after target cell injection. MataHari are shown in green and male targets in magenta. Scale bar, 20 μm.

Movie S4, related to Figure 6. Anti-PD-1 treatment has no detectable effect on T cell-target cell conjugation in syngeneic HSCT

Female recipients were transplanted with female bone marrow, MataHari CD8+ T cells (10% of GFP-expressing and 90% colorless T cells), and colorless polyclonal CD4+ T cells. On day 7 post-transplantation, mice received a single dose of either blocking anti-PD-1 antibody or an isotype control. CFP-expressing male splenocytes were injected 6h later. Two-photon imaging of popliteal lymph nodes was performed 12 hours after target cell injection. MataHari are shown in green and male targets in magenta. Scale bar, 20 μm.